

Chemical Composition and Phase Evolution in DMAI-Derived Inorganic Perovskite Solar Cells

Hongguang Meng,^{†,||,#} Zhipeng Shao,^{†,#} Li Wang,[‡] Zhipeng Li,[†] Ranran Liu,^{†,‡} Yingping Fan,^{†,‡} Guanglei Cui,^{*,†,§} and Shuping Pang^{*,†,§,||}

[†]Qingdao Institute of Bioenergy and Bioprocess Technology, Chinese Academy of Sciences, Qingdao 266101, People's Republic of China

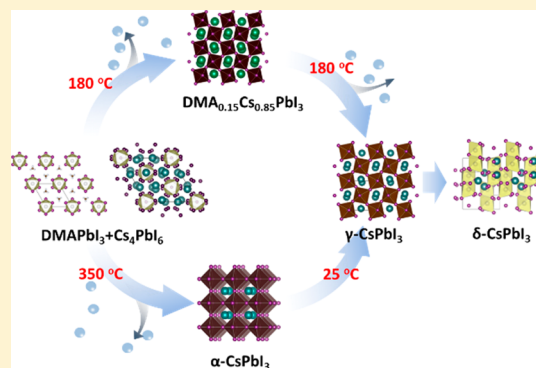
[‡]Qingdao University of Science and Technology, Qingdao 266042, People's Republic of China

[§]Dalian National Laboratory for Clean Energy, Dalian 116023, People's Republic of China

^{||}Center of Materials Science and Optoelectronics Engineering, University of Chinese Academy of Sciences, Beijing 100049, People's Republic of China

Supporting Information

ABSTRACT: Inorganic CsPbI₃ is promising to enhance the thermal stability of perovskite solar cells. The dimethylamine iodide (DMAI) derived method is currently the most efficient way to achieve high efficiency, but the effect of DMAI has not been fully explained. Herein, the chemical composition and phase evolution of the mixed DMAI/CsPbI₃ layer during thermal treatment has been studied. The results demonstrate that, with the common DMAI/CsI/PbI₂ recipe in DMSO solvent, a mixed perovskite DMA_{0.15}Cs_{0.85}PbI₃ is first formed through a solid reaction between DMAPbI₃ and Cs₄PbI₆. Further thermal treatment will transform the mixed perovskite phase directly to γ -CsPbI₃ and then spontaneously convert to δ -CsPbI₃. It has been also demonstrated that the DMA_{0.15}Cs_{0.85}PbI₃ phase is thermodynamically stable and shows a bandgap of 1.67 eV, which is narrower than 1.73 eV of γ -CsPbI₃. The device efficiency of the mixed DMA_{0.15}Cs_{0.85}PbI₃ perovskite is therefore highly improved in comparison with the pure inorganic γ -CsPbI₃ perovskite.



Cesium-based inorganic perovskite CsPbI₃ solar cells have attracted increasing research interests due to its improved thermal stability and reduced ion immigration in comparison with their organic–inorganic counterparts.^{1–4} However, the preferred black perovskite CsPbI₃ is thermodynamically unstable at room temperature, and it will spontaneously transform to the undesired nonphotoactive yellow phase (δ -phase).^{4–11}

The essence of the phase instability is the small size of the Cs cation, which is not suitable to support the three-dimensional PbI₃[−] framework.¹² The large lattice strain induced from the ion size mismatch will drive the CsPbI₃ lattice structure from three-dimensional (3D) perovskite phases to the one-dimensional (1D) nonperovskite phase. Therefore, the improvement of the lattice symmetry and reduction of the lattice strain are the two directions to dissolve the problem of phase instability.^{13–21} The nanocrystal-induced phase stabilization is one strategy to reduce the lattice strain by increasing the surface area of the crystals in the film, which is normally realized by introducing organic long-chain alkyl amine in the precursor solution.^{22,5} The shortcoming of this

method is its negative effect of a large number of grain boundaries on the carrier transport and injection. Currently, the most widely used and effective strategies are the DMAI-related methods,^{23–33} including the DMAI additive methods and the HI derived methods. The HI derived methods, normally named HI additive, HI-PbI₂, or HPbI₃ precursor, are demonstrated to inevitably bring the DMA byproduct in the precursor solution from the reaction between HI and DMF.^{34,35}

Although there are already several works focused on the elaboration of the final perovskite layer with the pure inorganic phase or still the organic–inorganic composite, the conclusion is still a huge controversy.^{31,34–38} Therefore, whether the organic DMA cation exists, how much of the organic DMA cation is in the crystal lattice, the properties of the DMA/Cs mixed perovskite phase, and even the phase evolution process

Received: October 17, 2019

Accepted: December 13, 2019

Published: December 17, 2019

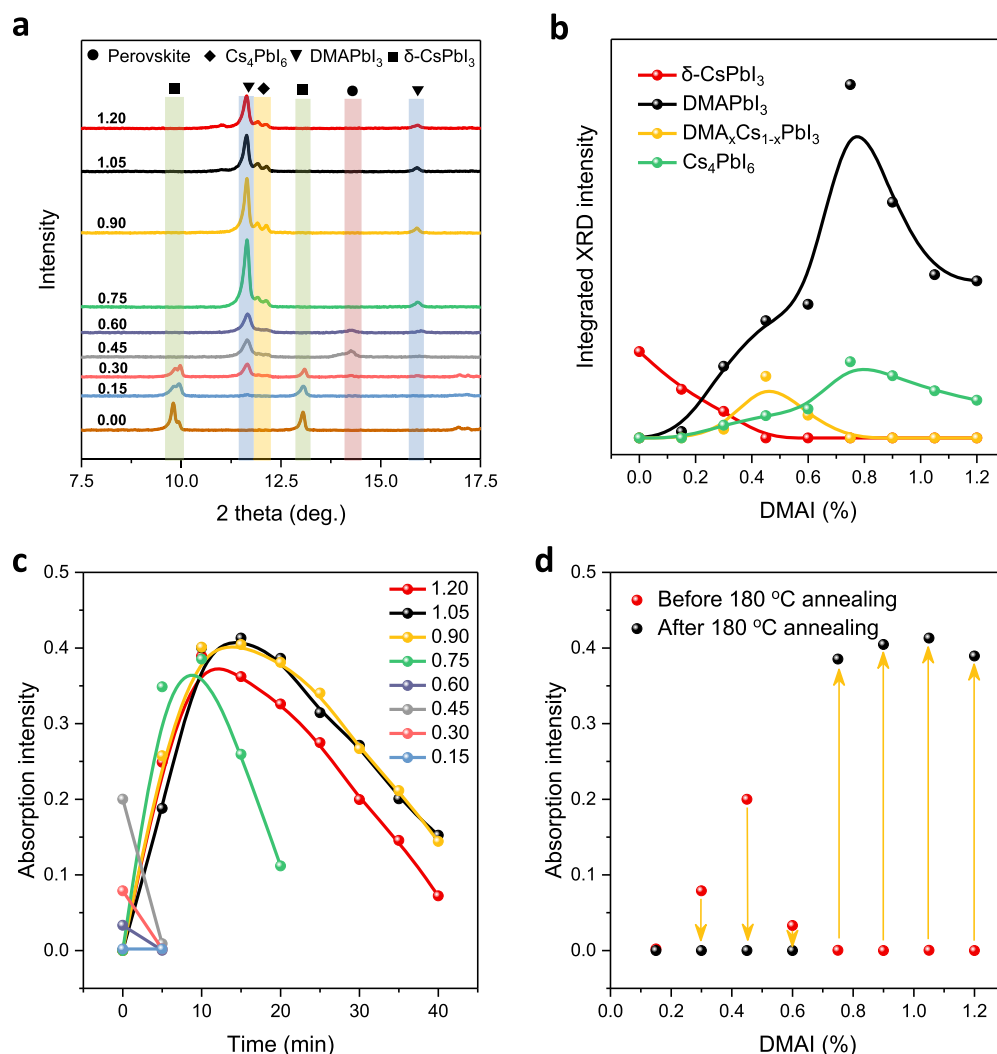


Figure 1. (a) XRD patterns of raw films with different mole ratios of DMAI/CsPbI₃ after heating at 100 °C for 10 min. (b) Integrated intensity of δ -CsPbI₃, DMA_xCs_{1-x}PbI₃, DMAPbI₃, and Cs₄PbI₆ phases in the raw films. (c) Absorption intensity evolution of the raw films heated at 180 °C for different times. (d) Absorption intensity of films before and after annealing at 180 °C. The absorption intensity was taken at 690 nm.

during the thermal treatment are urgently required to be carefully addressed.

In this work, we studied the chemical composition and phase evolution of the mixed DMAI/CsPbI₃ layer during thermal annealing. It was strongly evidenced that, with a DMAI/CsI/PbI₂ recipe, DMAPbI₃ and Cs₄PbI₆ were first formed and then transformed into mixed cation perovskite phase DMA_{0.15}Cs_{0.85}PbI₃. The mixed DMA_{0.15}Cs_{0.85}PbI₃ perovskite is thermodynamically stable, and it shows a narrower bandgap of 1.67 eV. It is also found that the more symmetrical DMA_{0.15}Cs_{0.85}PbI₃ perovskite phase exhibits an enhanced device efficiency compared to that of the γ -CsPbI₃ perovskite.

Prior to investigating the mechanism of the DMAI-assisted formation of the Cs base perovskite thin film, the stoichiometric ratio of DMAI/CsPbI₃ was first studied. The DMAI powder was directly added into the CsPbI₃ solution with mole ratios of DMAI/CsPbI₃ of 0.15, 0.30, 0.45, 0.60, 0.75, 0.90, 1.05, and 1.20. DMSO was used as a solvent in all following studies unless otherwise noted. The raw films were spin-coated and annealed at 100 °C for 10 min. Figure 1a shows a series of XRD patterns of the raw films, and it is found that the phases in each condition are strictly dependent on the

DMAI content. We index all of the diffraction peaks to four phases of δ -CsPbI₃, DMA_xCs_{1-x}PbI₃, DMAPbI₃, and Cs₄PbI₆.^{10,11,39–42} The XRD spectra of DMAPbI₃ and Cs₄PbI₆ films are also studied, as shown in Figure S1 for reference. Only the samples with DMAI/CsPbI₃ ratios of around 0.45 have the darkest color owing to the formation of a certain amount of mixed DMA_xCs_{1-x}PbI₃ perovskite phase, while all other samples are yellow or colorless, as illustrated in Figure S2. To intuitively describe the variation of the four phases in each condition, the integrated intensities of the diffraction peaks of δ -CsPbI₃ (13.0°), DMA_xCs_{1-x}PbI₃ (14.3°), DMAPbI₃ (11.6°), and Cs₄PbI₆ (11.9° and 12.1°) are plotted in Figure 1b. Without DMAI additive, a δ -CsPbI₃ phase is formed. The increase of DMAI content from 0 to 0.45 induces the formation of DMAPbI₃, mixed perovskite DMA_xCs_{1-x}PbI₃, and the Cs-rich phase Cs₄PbI₆. Further increase in the DMAI content efficiently restricts the formation of the mixed DMA_xCs_{1-x}PbI₃ perovskites, and the films change to colorless (Figure S2). In the high DMAI content stage with DMAI/CsPbI₃ \geq 0.75, the phases in the films are mainly DMAPbI₃ and Cs₄PbI₆.

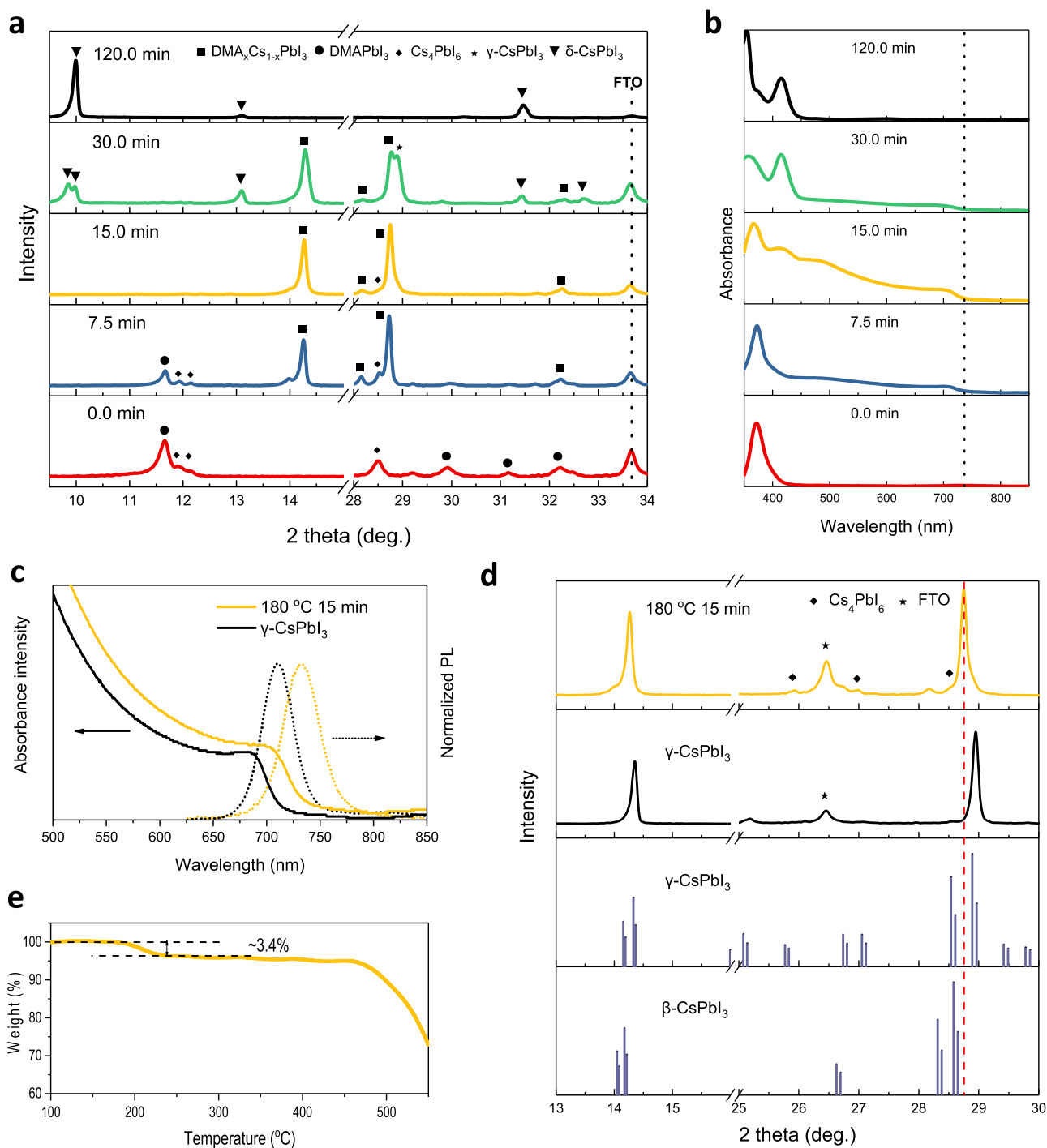


Figure 2. (a) XRD patterns and (b) UV-vis spectra of DMAI/CsPbI₃ films annealed at 180 °C for different times. (c) Steady PL and absorption spectra and (d) XRD patterns of DMAI/CsPbI₃ films annealed at 180 °C for 15 min and γ-CsPbI₃ films. The γ-CsPbI₃ films were fabricated by annealing at 350 °C for 15 min. (e) TG measurement of the DMAI/CsPbI₃ powder annealed at 180 °C for 15 min.

The XRD patterns of the DMAI/CsPbI₃ (DMAI/CsPbI₃ = 1) films heated at 180 °C for different times were measured as presented in Figure 2a. Before annealing, the peaks at 11.6 and 32.2° can be indexed to DMAPbI₃ with an orthorhombic (space group $P6_3mc$) structure, consisting of arrays of 1D face-shared [PbI₆⁴⁺]_n octahedra with intercalated DMA cations for charge balance.³⁴ Other weaker diffraction peaks at 11.9, 12.1, and 28.6° indicate the presence of Cs-rich phase Cs₄PbI₆. Further annealing induces a solid-state reaction between DMAPbI₃ and Cs₄PbI₆ to form a mixed perovskite phase of

DMA_xCs_{1-x}PbI₃ with the diffraction peaks at 14.2 and 28.7°, which are the features of the 3D corner-shared [PbI₆⁴⁻]_n perovskite framework. It is interesting that the diffraction peaks of the mixed cation perovskite remain constant in the whole annealing process. The film heated for 15 min gives the highest diffraction peak of the perovskite phase, and the DMAPbI₃ phase completely disappears. We also see some weak diffraction peaks at 24.0, 26.0, 27.0, and 28.6°, which belong to Cs₄PbI₆, as marked in Figure 2a. Additionally, other conditions of using DMF as the solvent or heating the films in

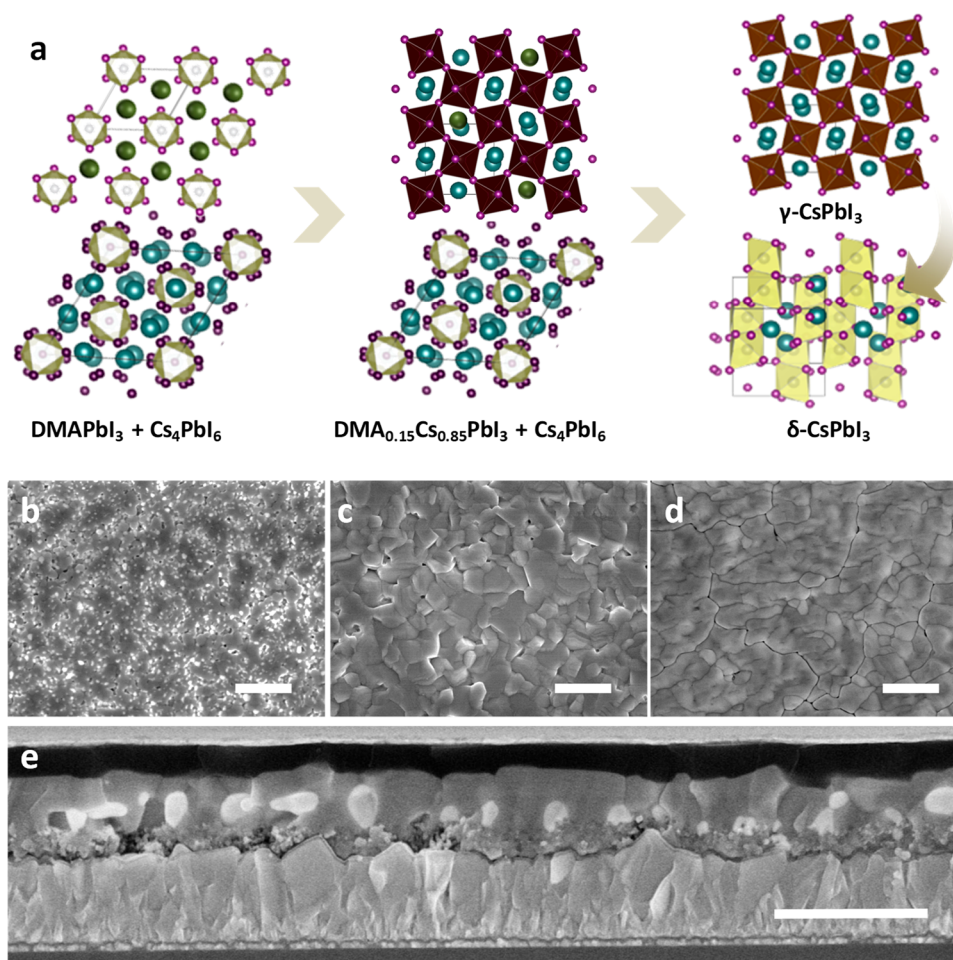


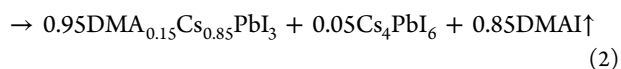
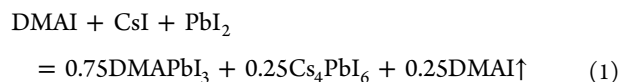
Figure 3. (a) Crystal structure evolution during the film fabrication. (b–d) SEM images of DMAI/CsPbI₃ films annealed at 180 °C for 0, 15, and 120 min, respectively. (e) Cross-sectional SEM image of the film heated for 15 min. Scale bars are 1 μm .

air were studied, and the Cs_4PbI_6 peaks also appear as shown in Figures S3 and S4, indicating the independence of the solvents. Upon further increase of the annealing time to 30 min, the $\gamma\text{-CsPbI}_3$ phase appears, and the film totally transforms into the yellow $\delta\text{-CsPbI}_3$ phase in 120 min.

The corresponding UV–vis spectra in Figure 2b present similar results as those discussed above. The absorption peak of the raw film at 373 nm is owed to the absorption of combined DMAPI_3 (380 nm) and Cs_4PbI_6 (370 nm), as evidenced in Figure S5. The absorption onset of $\text{DMA}_x\text{Cs}_{1-x}\text{PbI}_3$ perovskite remains constant at 740 nm, which also suggests that the x here is fixed, not a variable. The UV–vis spectra of $\text{DMA}_x\text{Cs}_{1-x}\text{PbI}_3$ perovskite film (180°C , 15 min) give a 25 nm red shift in comparison with that of $\gamma\text{-CsPbI}_3$ (350°C , 15 min), as shown in Figure 2c. The E_g^{opt} of $\text{DMA}_{0.15}\text{Cs}_{0.85}\text{PbI}_3$ is calculated to be 1.67 eV and is much narrower than 1.73 eV of $\gamma\text{-CsPbI}_3$. The red shift was also proved in their steady PL spectra, as shown in Figure 2c. Figure 2d shows the XRD patterns of $\text{DMA}_x\text{Cs}_{1-x}\text{PbI}_3$ and $\gamma\text{-CsPbI}_3$ films. The as-prepared $\text{DMA}_x\text{Cs}_{1-x}\text{PbI}_3$ is more like a γ -phase perovskite. The left shift of the (220) diffraction peak in comparison with pure $\gamma\text{-CsPbI}_3$ indicates the enlarged d -spacing. It was calculated that the unit cell volume is $978\ \text{\AA}^3$ with $a = 8.87\ \text{\AA}$, $b = 8.71\ \text{\AA}$, and $c = 12.67\ \text{\AA}$ for $\text{DMA}_x\text{Cs}_{1-x}\text{PbI}_3$, which is slightly larger than $953\ \text{\AA}^3$ of $\gamma\text{-CsPbI}_3$. The enlarged unit cell volume could result from an incorporated larger size DMA cation in the crystal lattice.^{43,44}

To quantify how much DMA cation remains in the crystal lattice, the TG curves of the DMAI/CsPbI₃ and the $\text{DMA}_x\text{Cs}_{1-x}\text{PbI}_3$ perovskite (180°C , 15 min) were checked, as presented in Figures S6 and 2e. The powder samples were collected from the films after the thermal treatments. For the DMAI/CsPbI₃ sample, there is about 18.5% weight loss from 200 to 450°C , which is almost the same amount as the initial DMAI added (Figure S6). The powder sample after annealing at 180°C for 15 min shows a 3.4% weight loss in the same temperature range (Figure 2e). Thus, the formula of the mixed perovskite could be calculated to be $\text{DMA}_{0.15}\text{Cs}_{0.85}\text{PbI}_3$, and the mole ratio of $\text{DMA}_{0.15}\text{Cs}_{0.85}\text{PbI}_3$ to Cs_4PbI_6 is 20:1. The detailed calculation is given in the Supporting Information.

Summarizing the above XRD and TG results, we can get the following equations:



The processes of DMAI-assisted film formation could be summarized as follows. After spin-coating and thermal

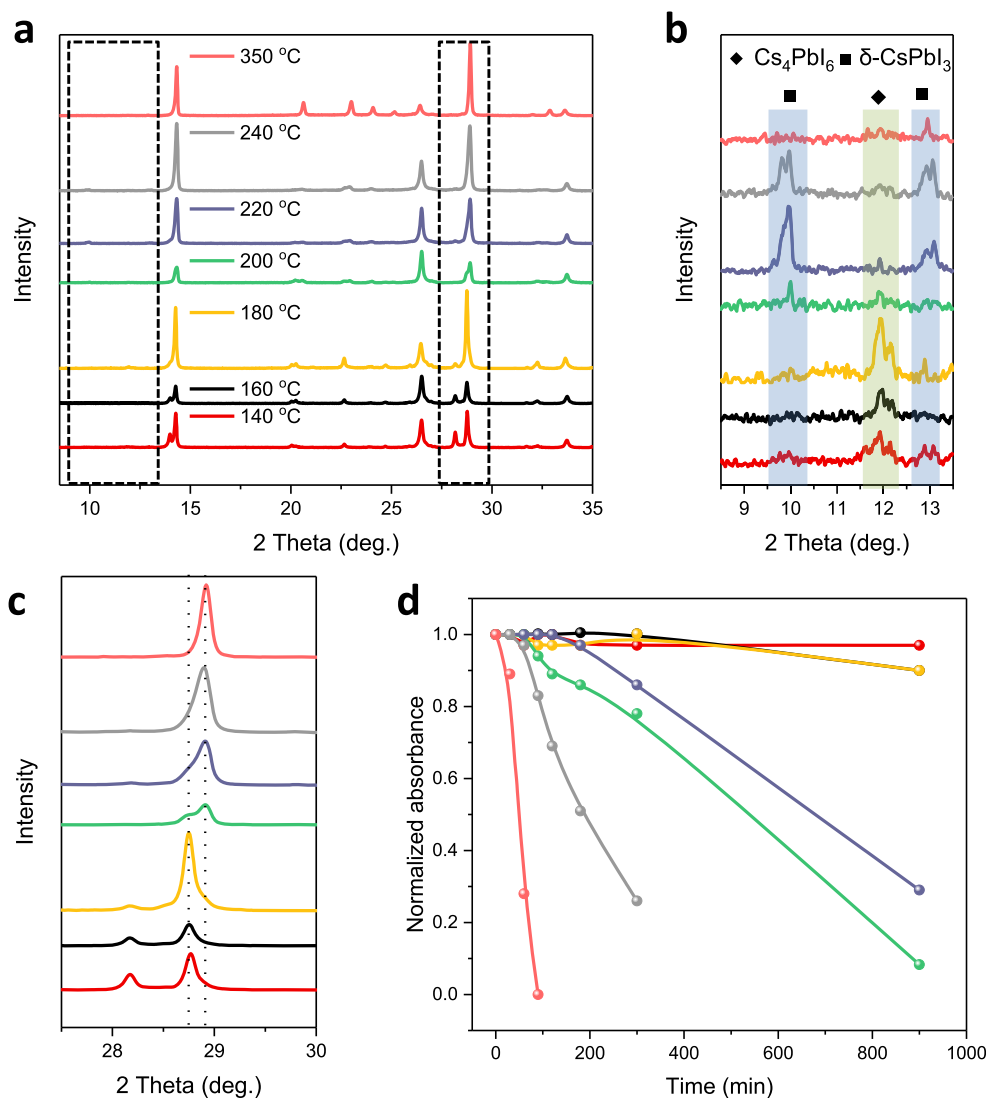


Figure 4. (a–c) XRD patterns of the DMAI/CsPbI₃ films annealed at different temperatures. (d) Evolution of the absorbance of the above films at a wavelength of 670 nm as a function of time in air under high humidity of 70–80%.

annealing at 100 °C for 10 min, DMAPbI₃ and Cs₄PbI₆ phases are first formed in the film (reaction 1). When the film is annealed at 180 °C for 15 min, the film transforms into a mixed perovskite phase of DMA_{0.15}Cs_{0.85}PbI₃ with a certain amount of Cs₄PbI₆ residue (reaction 2). Further extending the thermal annealing time, the mixed perovskite DMA_{0.15}Cs_{0.85}PbI₃ directly converts to γ -CsPbI₃ and then spontaneously converts to δ -CsPbI₃ (reactions 3 and 4) due to the metastable property of γ -CsPbI₃ at low temperature. The phase evolution and crystal structures of DMAPbI₃, Cs₄PbI₆, DMA_{0.15}Cs_{0.85}PbI₃, γ -CsPbI₃, and δ -CsPbI₃ are illustrated in Figure 3a. Because of the instability of the γ -CsPbI₃, δ -CsPbI₃ appears simultaneously in the films. For the ABX₃ perovskite phase, the Goldschmidt's tolerance factor (TF) is presented as $t = (r_A + r_X) / \sqrt{2}(r_B + r_X)$, in which r_A , r_B , and r_X are the ionic radii of A, B, and X, respectively. The calculated TF of CsPbI₃ is 0.85, and the TF of DMAPbI₃ should be 1.03.³⁴ The alloying of the Cs and DMA cations with a ratio of 0.15/0.85 could form a more stable perovskite phase and give a TF of 0.88. In the following discussion, the DMAI/CsPbI₃ film heated at 180 °C for 15 min is named DMA_{0.15}Cs_{0.85}PbI₃. It is worth noting that the phase stability of the mixed DMA_{0.15}Cs_{0.85}PbI₃

perovskite phase is highly improved, as evidenced in Figure S7. For the pure inorganic γ -CsPbI₃, it will quickly transform to the δ -CsPbI₃ at 120 °C, while the DMA_{0.15}Cs_{0.85}PbI₃ film shows no obvious change for 300 min.

As shown in Figure 3b, a very smooth DMAI/CsPbI₃ raw film could be easily obtained by spin coating. After heating at 180 °C for 15 min, the film gradually changes to the mixed DMA_{0.15}Cs_{0.85}PbI₃ perovskite phase with a mean grain size of 400 nm (Figure S8). According to eq 2, there should be a small amount of Cs₄PbI₆ phase left in the film. As shown in the cross-sectional SEM image in Figure 3e, the white particles with a size of about 50 nm are supposed to be Cs₄PbI₆, which are embedded inside of the perovskite films. It is also found that the phase transition from mixed DMA_{0.15}Cs_{0.85}PbI₃ perovskite to γ -CsPbI₃ and δ -CsPbI₃ is not homogeneous; on the contrary, it starts from a point, then gradually expands, and finally completely fades into a light-yellow film (Figures S9 and S10). The morphology of the δ -CsPbI₃ film is shown in Figure 3d.

To reveal the influence of temperature on the phase evolution process, XRD patterns and UV–vis spectra of DMAI/CsPbI₃ films annealed at different temperatures were

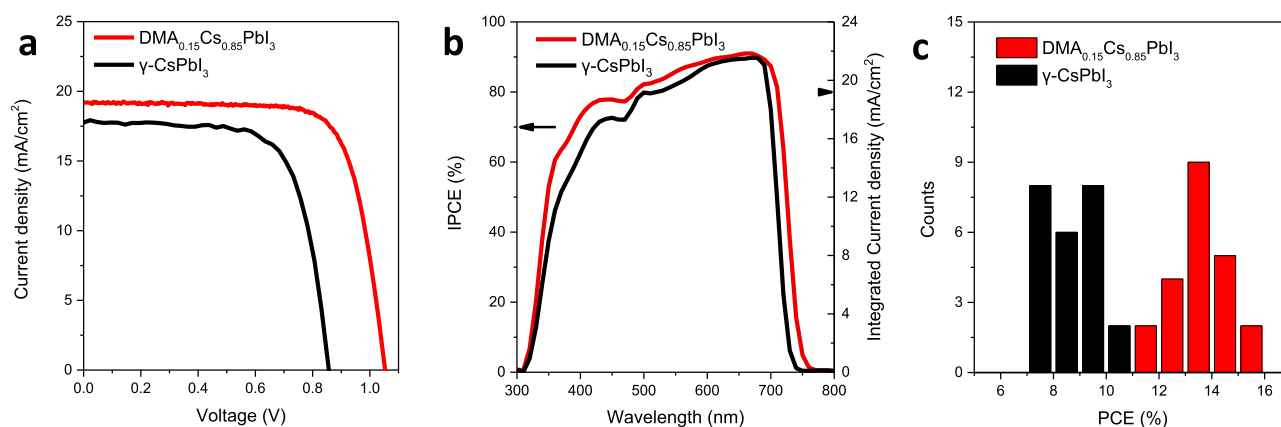


Figure 5. (a) J - V curves, (b) IPCE spectra, and (c) the PCE distribution of the DMA_{0.15}Cs_{0.85}PbI₃ and γ -CsPbI₃ solar cells.

studied as presented in Figures 4 and S11. For each annealing temperature, the heating time is optimized according to the UV-vis results. The annealing time is 180, 45, 15, 10, 4, and 1.5 min for 140, 160, 180, 200, 220, and 240 °C, respectively. When the annealing temperature is lower than 180 °C, Cs₄PbI₆ peaks at 2θ of 11.9 and 12.1° are observed, and they decrease when the temperature exceeds 200 °C, as exhibited in Figure 4b. At 180 °C, the sample shows the highest (002) diffraction peak of a mixed DMA_{0.15}Cs_{0.85}PbI₃ perovskite phase, suggesting the enhanced crystallization. Once the annealing temperature exceeds 200 °C, the sample shows a main peak at $2\theta = 28.95^\circ$ and a shoulder peak at $2\theta = 28.75^\circ$ due to the formation of the mixed compounds of γ -CsPbI₃ ($2\theta = 28.95^\circ$) perovskites and a small number of DMA_{0.15}Cs_{0.85}PbI₃ ($2\theta = 28.75^\circ$). The fraction of DMA_{0.15}Cs_{0.85}PbI₃ decreases as the temperature increases from 200 to 240 °C. The appearance of δ -CsPbI₃ ($2\theta = 9.8$ and 13.0° , Figure 2b) at higher temperatures is supposed due to the slight phase transformation from γ -CsPbI₃.

Figure 4d shows the moisture stability by tracing the absorption intensity. These films were kept in air under a high relative humidity of 70–80%. There is negligible degradation observed for the DMA_{0.15}Cs_{0.85}PbI₃ films (140, 160, and 180 °C) after 900 min, while the γ -CsPbI₃ fully degraded into δ -CsPbI₃ in less than 90 min. Moreover, the DMA_{0.15}Cs_{0.85}PbI₃ films exhibited excellent phase stability in dry air; they showed no degradation in 3 months in humidity of around 10%, as shown in Figure S12.

We finally fabricated solar cells with DMA_{0.15}Cs_{0.85}PbI₃ as the photoactive layer in the device structure of FTO/C-TiO₂/P-TiO₂/perovskite/spiro-OMeTAD/Ag. For comparison, the γ -CsPbI₃ solar cells were assembled as well. The detailed fabrication processes are listed in the Experimental Section. The champion PCE of the mixed perovskite DMA_{0.15}Cs_{0.85}PbI₃ could reach 15.3% with J_{sc} of 19.4 mA/cm², V_{oc} of 1.05 V, and FF of 0.75, while the pure inorganic γ -CsPbI₃ solar cell gave a lower PCE of 10.7%, J_{sc} of 17.9 mA/cm², V_{oc} of 0.86 V, and FF of 0.70. Also, both devices showed good reproducibility (Figure 5c). As shown in the IPCE spectra (Figure 5b), the integrated photocurrent density was calculated to be 18.8 mA/cm² for DMA_{0.15}Cs_{0.85}PbI₃ solar cells and 17.0 mA/cm² for γ -CsPbI₃ solar cells, which was mainly because of the widened optical absorption range. The hysteresis property of the champion mixed perovskite was studied with reverse and forward scan; the results are shown in Figure S13. Maximum power point tracking gives a stabilized PCE of 14.4%. It should

be noted that there is a smaller amount of Cs₄PbI₆ embedded in the DMA_{0.15}Cs_{0.85}PbI₃ film, and the effect of the Cs₄PbI₆ on the device performance is still not clear and needs to be further investigated.

In summary, to unveil the effect and function of DMAI in preparing the inorganic perovskite devices, we tracked the chemical composition, phase, and bandgap of the perovskite layer during the thermal treatment. It was found that, with a controlled thermal annealing process, a more thermodynamically stable perovskite of mixed cation DMA_{0.15}Cs_{0.85}PbI₃ could form with a certain amount of Cs₄PbI₆ residue. Unlike other mixed cation perovskite materials, the composition of DMA/Cs mixed perovskite is well fixed instead of a continuous component distribution. Further thermal annealing transformed the film into γ -CsPbI₃ and then into δ -CsPbI₃. The DMA_{0.15}Cs_{0.85}PbI₃ phase exhibits a more symmetrical structure, a narrower bandgap, and superior phase stability than that of γ -CsPbI₃. These findings will benefit the in-depth understanding of the properties of inorganic perovskite and their phase stability issue.

■ ASSOCIATED CONTENT

Supporting Information

The Supporting Information is available free of charge at <https://pubs.acs.org/doi/10.1021/acsenerylett.9b02272>.

Experimental section and additional characterization and analysis data for the perovskite films and PSCs, including XRD spectra and patterns, normalized absorption spectra, TG curves, grain size statistics, SEM images, UV-vis spectra, hysteresis properties, and maximum power point tracking (PDF)

■ AUTHOR INFORMATION

Corresponding Authors

*E-mail: cui@qibebt.ac.cn (G.C.).

*E-mail: pangsp@qibebt.ac.cn (S.P.).

ORCID

Guanglei Cui: 0000-0001-5987-7569

Shuping Pang: 0000-0002-2526-4104

Author Contributions

#H.M. and Z.S. contributed equally.

Notes

The authors declare no competing financial interest.

ACKNOWLEDGMENTS

S.P. acknowledges the support of the Dalian National Laboratory for Clean Energy, CAS (DICP&QIBEBT UN201705), the DNL Cooperation Fund, CAS (DNL180311), and the Taishan Scholar Project of Shandong Province. G.C. acknowledges the support of the Major Program of Shandong Province Natural Science Foundation (ZR2018ZB0316) and the Qingdao Key Lab of Solar Energy Utilization & Energy Storage Technology. Z.S. acknowledges the support of the National Natural Science Foundation of China (51902324)

REFERENCES

- (1) Sutton, R. J.; Eperon, G. E.; Miranda, L.; Parrott, E. S.; Kamino, B. A.; Patel, J. B.; Hörantner, M. T.; Johnston, M. B.; Haghighirad, A. A.; Moore, D. T.; Snaith, H. J. Bandgap-Tunable Cesium Lead Halide Perovskites with High Thermal Stability for Efficient Solar Cells. *Adv. Energy Mater.* **2016**, *6*, 1502458.
- (2) Zhou, W.; Zhao, Y.; Zhou, X.; Fu, R.; Li, Q.; Zhao, Y.; Liu, K.; Yu, D.; Zhao, Q. Light-Independent Ionic Transport in Inorganic Perovskite and Ultrastable Cs-Based Perovskite Solar Cells. *J. Phys. Chem. Lett.* **2017**, *8*, 4122–4128.
- (3) Eperon, G. E.; Paternò, G. M.; Sutton, R. J.; Zampetti, A.; Haghighirad, A. A.; Cacialli, F.; Snaith, H. J. Inorganic caesium lead iodide perovskite solar cells. *J. Mater. Chem. A* **2015**, *3*, 19688–19695.
- (4) Zhou, Y.; Zhao, Y. Chemical stability and instability of inorganic halide perovskites. *Energy Environ. Sci.* **2019**, *12*, 1495–1511.
- (5) Swarnkar, A.; Marshall, A. R.; Sanehira, E. M.; Chernomordik, B. D.; Moore, D. T.; Christians, J. A.; Chakrabarti, T.; Luther, J. M. Quantum dot-induced phase stabilization of alpha-CsPbI₃ perovskite for high-efficiency photovoltaics. *Science* **2016**, *354*, 92–95.
- (6) Liang, J.; Wang, C.; Wang, Y.; Xu, Z.; Lu, Z.; Ma, Y.; Zhu, H.; Hu, Y.; Xiao, C.; Yi, X.; Zhu, G.; Lv, H.; Ma, L.; Chen, T.; Tie, Z.; Jin, Z.; Liu, J. All-Inorganic Perovskite Solar Cells. *J. Am. Chem. Soc.* **2016**, *138*, 15829–15832.
- (7) Beal, R. E.; Slotcavage, D. J.; Leijtens, T.; Bowring, A. R.; Belisle, R. A.; Nguyen, W. H.; Burkhard, G. F.; Hoke, E. T.; McGehee, M. D. Cesium Lead Halide Perovskites with Improved Stability for Tandem Solar Cells. *J. Phys. Chem. Lett.* **2016**, *7*, 746–51.
- (8) Wang, Q.; Zheng, X.; Deng, Y.; Zhao, J.; Chen, Z.; Huang, J. Stabilizing the α -Phase of CsPbI₃ Perovskite by Sulfobetaine Zwitterions in One-Step Spin-Coating Films. *Joule* **2017**, *1*, 371–382.
- (9) Kye, Y.-H.; Yu, C.-J.; Jong, U.-G.; Ri, K.-C.; Kim, J.-S.; Choe, S.-H.; Hong, S.-N.; Li, S.; Wilson, J. N.; Walsh, A. Vacancy-Driven Stabilization of the Cubic Perovskite Polymorph of CsPbI₃. *J. Phys. Chem. C* **2019**, *123*, 9735–9744.
- (10) Marronnier, A.; Roma, G.; Boyer-Richard, S.; Pedesseau, L.; Jancu, J. M.; Bonnassieux, Y.; Katan, C.; Stoumpos, C. C.; Kanatzidis, M. G.; Even, J. Anharmonicity and Disorder in the Black Phases of Cesium Lead Iodide Used for Stable Inorganic Perovskite Solar Cells. *ACS Nano* **2018**, *12*, 3477–3486.
- (11) Sutton, R. J.; Filip, M. R.; Haghighirad, A. A.; Sakai, N.; Wenger, B.; Giustino, F.; Snaith, H. J. Cubic or Orthorhombic? Revealing the Crystal Structure of Metastable Black-Phase CsPbI₃ by Theory and Experiment. *ACS Energy Lett.* **2018**, *3*, 1787–1794.
- (12) Swarnkar, A.; Mir, W. J.; Nag, A. Can B-Site Doping or Alloying Improve Thermal- and Phase-Stability of All-Inorganic CsPbX₃ (X = Cl, Br, I) Perovskites? *ACS Energy Lett.* **2018**, *3*, 286–289.
- (13) Jiang, Y.; Yuan, J.; Ni, Y.; Yang, J.; Wang, Y.; Jiu, T.; Yuan, M.; Chen, J. Reduced-Dimensional α -CsPbX₃ Perovskites for Efficient and Stable Photovoltaics. *Joule* **2018**, *2*, 1356–1368.
- (14) Xiang, W.; Wang, Z.; Kubicki, D. J.; Tress, W.; Luo, J.; Prochowicz, D.; Akin, S.; Emsley, L.; Zhou, J.; Dietler, G.; Grätzel, M.; Hagfeldt, A. Europium-Doped CsPbI₂Br for Stable and Highly Efficient Inorganic Perovskite Solar Cells. *Joule* **2019**, *3*, 205–214.
- (15) Zhang, T. Y.; Dar, M. I.; Li, G.; Xu, F.; Guo, N. J.; Grätzel, M.; Zhao, Y. X. Bication lead iodide 2D perovskite component to stabilize inorganic alpha-CsPbI₃ perovskite phase for high-efficiency solar cells. *Sci. Adv.* **2017**, *3*, No. e1700841.
- (16) Zhang, J.; Yang, L.; Zhong, Y.; Hao, H.; Yang, M.; Liu, R. Improved phase stability of the CsPbI₃ perovskite via organic cation doping. *Phys. Chem. Chem. Phys.* **2019**, *21*, 11175–11180.
- (17) Ye, Q.; Zhao, Y.; Mu, S.; Gao, P.; Zhang, X.; You, J. Stabilizing the black phase of cesium lead halide inorganic perovskite for efficient solar cells. *Sci. China: Chem.* **2019**, *62*, 810–821.
- (18) Ding, X.; Chen, H.; Wu, Y.; Ma, S.; Dai, S.; Yang, S.; Zhu, J. Triple cation additive NH₃⁺C₂H₄NH₂⁺C₂H₄NH₃⁺-induced phase-stable inorganic α -CsPbI₃ perovskite films for use in solar cells. *J. Mater. Chem. A* **2018**, *6*, 18258–18266.
- (19) Fu, Y.; Rea, M. T.; Chen, J.; Morrow, D. J.; Hautzinger, M. P.; Zhao, Y.; Pan, D.; Manger, L. H.; Wright, J. C.; Goldsmith, R. H.; Jin, S. Selective Stabilization and Photophysical Properties of Metastable Perovskite Polymorphs of CsPbI₃ in Thin Films. *Chem. Mater.* **2017**, *29*, 8385–8394.
- (20) Jena, A. K.; Kulkarni, A.; Sanehira, Y.; Ikegami, M.; Miyasaka, T. Stabilization of α -CsPbI₃ in Ambient Room Temperature Conditions by Incorporating Eu into CsPbI₃. *Chem. Mater.* **2018**, *30*, 6668–6674.
- (21) Ding, J.; Du, S.; Zuo, Z.; Zhao, Y.; Cui, H.; Zhan, X. High Detectivity and Rapid Response in Perovskite CsPbBr₃ Single-Crystal Photodetector. *J. Phys. Chem. C* **2017**, *121*, 4917–4923.
- (22) Xue, J.; Lee, J.-W.; Dai, Z.; Wang, R.; Nuryeva, S.; Liao, M. E.; Chang, S.-Y.; Meng, L.; Meng, D.; Sun, P.; Lin, O.; Goorsky, M. S.; Yang, Y. Surface Ligand Management for Stable FAPbI₃ Perovskite Quantum Dot Solar Cells. *Joule* **2018**, *2*, 1866–1878.
- (23) Haque, F.; Wright, M.; Mahmud, M. A.; Yi, H.; Wang, D.; Duan, L.; Xu, C.; Upama, M. B.; Uddin, A. Effects of Hydroiodic Acid Concentration on the Properties of CsPbI₃ Perovskite Solar Cells. *ACS Omega* **2018**, *3*, 11937–11944.
- (24) Wang, K.; Jin, Z.; Liang, L.; Bian, H.; Bai, D.; Wang, H.; Zhang, J.; Wang, Q.; Liu, S. All-inorganic cesium lead iodide perovskite solar cells with stabilized efficiency beyond 15%. *Nat. Commun.* **2018**, *9*, 4544.
- (25) Xiang, S.; Li, W.; Wei, Y.; Liu, J.; Liu, H.; Zhu, L.; Yang, S.; Chen, H. Sodium Doping Pushes the Efficiency of Carbon-Based CsPbI₃ Perovskite Solar Cells to 10.7%. *iScience* **2019**, *15*, 156–164.
- (26) Xiang, S.; Fu, Z.; Li, W.; Wei, Y.; Liu, J.; Liu, H.; Zhu, L.; Zhang, R.; Chen, H. Highly Air-Stable Carbon-Based α -CsPbI₃ Perovskite Solar Cells with a Broadened Optical Spectrum. *ACS Energy Lett.* **2018**, *3*, 1824–1831.
- (27) Wang, K.; Jin, Z.; Liang, L.; Bian, H.; Wang, H.; Feng, J.; Wang, Q.; Liu, S. Chlorine doping for black γ -CsPbI₃ solar cells with stabilized efficiency beyond 16%. *Nano Energy* **2019**, *58*, 175–182.
- (28) Liang, L.; Liu, M.; Jin, Z.; Wang, Q.; Wang, H.; Bian, H.; Shi, F.; Liu, S. Optical Management with Nanoparticles for a Light Conversion Efficiency Enhancement in Inorganic gamma-CsPbI₃ Solar Cells. *Nano Lett.* **2019**, *19*, 1796–1804.
- (29) Zhao, B.; Jin, S. F.; Huang, S.; Liu, N.; Ma, J. Y.; Xue, D. J.; Han, Q.; Ding, J.; Ge, Q. Q.; Feng, Y.; Hu, J. S. Thermodynamically Stable Orthorhombic gamma-CsPbI₃ Thin Films for High-Performance Photovoltaics. *J. Am. Chem. Soc.* **2018**, *140*, 11716–11725.
- (30) Wang, Y.; Zhang, T.; Kan, M.; Zhao, Y. Bifunctional Stabilization of All-Inorganic alpha-CsPbI₃ Perovskite for 17% Efficiency Photovoltaics. *J. Am. Chem. Soc.* **2018**, *140*, 12345–12348.
- (31) Wang, Y.; Zhang, T.; Kan, M.; Li, Y.; Wang, T.; Zhao, Y. Efficient α -CsPbI₃ Photovoltaics with Surface Terminated Organic Cations. *Joule* **2018**, *2*, 2065–2075.
- (32) Heo, D. Y.; Han, S. M.; Woo, N. S.; Kim, Y. J.; Kim, T.-Y.; Luo, Z.; Kim, S. Y. Role of Additives on the Performance of CsPbI₃ Solar Cells. *J. Phys. Chem. C* **2018**, *122*, 15903–15910.
- (33) Wang, K.; Li, Z.; Zhou, F.; Wang, H.; Bian, H.; Zhang, H.; Wang, Q.; Jin, Z.; Ding, L.; Liu, S. Ruddlesden–Popper 2D Component to Stabilize γ -CsPbI₃ Perovskite Phase for Stable and Efficient Photovoltaics. *Adv. Energy Mater.* **2019**, *9*, 1902529.

(34) Ke, W.; Spanopoulos, I.; Stoumpos, C. C.; Kanatzidis, M. G. Myths and reality of HPbI₃ in halide perovskite solar cells. *Nat. Commun.* **2018**, *9*, 4785.

(35) Pei, Y.; Liu, Y.; Li, F.; Bai, S.; Jian, X.; Liu, M. Unveiling Property of Hydrolysis-Derived DMAPbI₃ for Perovskite Devices: Composition Engineering, Defect Mitigation, and Stability Optimization. *iScience* **2019**, *15*, 165–172.

(36) Wu, T.; Wang, Y.; Dai, Z.; Cui, D.; Wang, T.; Meng, X.; Bi, E.; Yang, X.; Han, L. Efficient and Stable CsPbI₃ Solar Cells via Regulating Lattice Distortion with Surface Organic Terminal Groups. *Adv. Mater.* **2019**, *31*, No. 1900605.

(37) Wang, Y.; Dar, M. I.; Ono, L. K.; Zhang, T.; Kan, M.; Li, Y.; Zhang, L.; Wang, X.; Yang, Y.; Gao, X.; Qi, Y.; Grätzel, M.; Zhao, Y. Thermodynamically stabilized β -CsPbI₃-based perovskite solar cells with efficiencies > 18%. *Science* **2019**, *365*, 591–595.

(38) Wang, Y.; Liu, X.; Zhang, T.; Wang, X.; Kan, M.; Shi, J.; Zhao, Y. The Role of Dimethylammonium Iodine in CsPbI₃ Perovskite Fabrication: Additive or Dopant? *Angew. Chem., Int. Ed.* **2019**, *58*, 16691.

(39) Akkerman, Q. A.; Park, S.; Radicchi, E.; Nunzi, F.; Mosconi, E.; De Angelis, F.; Brescia, R.; Rastogi, P.; Prato, M.; Manna, L. Nearly Monodisperse Insulator Cs₄PbX₆ (X = Cl, Br, I) Nanocrystals, Their Mixed Halide Compositions, and Their Transformation into CsPbX₃ Nanocrystals. *Nano Lett.* **2017**, *17*, 1924–1930.

(40) Frolova, L. A.; Chang, Q.; Luchkin, S. Y.; Zhao, D.; Akbulatov, A. F.; Dremova, N. N.; Ivanov, A. V.; Chia, E. E. M.; Stevenson, K. J.; Troshin, P. A. Efficient and stable all-inorganic perovskite solar cells based on nonstoichiometric Cs_xPbI₂Br_x ($x > 1$) alloys. *J. Mater. Chem. C* **2019**, *7*, 5314–5323.

(41) Luo, P.; Xia, W.; Zhou, S.; Sun, L.; Cheng, J.; Xu, C.; Lu, Y. Solvent Engineering for Ambient-Air-Processed, Phase-Stable CsPbI₃ in Perovskite Solar Cells. *J. Phys. Chem. Lett.* **2016**, *7*, 3603–8.

(42) Garcia-Fernandez, A.; Bermudez-Garcia, J. M.; Castro-Garcia, S.; Llamas-Saiz, A. L.; Artiaga, R.; Lopez-Beceiro, J.; Hu, S.; Ren, W.; Stroppa, A.; Sanchez-Andujar, M.; Senaris-Rodriguez, M. A. Phase Transition, Dielectric Properties, and Ionic Transport in the [(CH₃)₂NH₂]PbI₃ Organic-Inorganic Hybrid with 2H-Hexagonal Perovskite Structure. *Inorg. Chem.* **2017**, *56*, 4918–4927.

(43) Lee, J.-W.; Kim, D.-H.; Kim, H.-S.; Seo, S.-W.; Cho, S. M.; Park, N.-G. Formamidinium and Cesium Hybridization for Photo- and Moisture-Stable Perovskite Solar Cell. *Adv. Energy Mater.* **2015**, *5*, 1501310.

(44) Tang, Z.; Bessho, T.; Awai, F.; Kinoshita, T.; Maitani, M. M.; Jono, R.; Murakami, T. N.; Wang, H.; Kubo, T.; Uchida, S.; Segawa, H. Hysteresis-free perovskite solar cells made of potassium-doped organometal halide perovskite. *Sci. Rep.* **2017**, *7*, 12183.